ACS APPLIED MATERIALS & INTERFACES

Research Article

www.acsami.org

Filtration-Based Synthesis of Micelle-Derived Composite Membranes for High-Flux Ultrafiltration

Xueping Yao,[†] Leiming Guo,[†] Xiaoqiang Chen,[†] Jun Huang,[†] Martin Steinhart,*[,‡] and Yong Wang*[,†]

[†]State Key Laboratory of Materials-Oriented Chemical Engineering, College of Chemistry and Chemical Engineering, Nanjing Tech University (formerly Nanjing University of Technology), Nanjing, 210009 Jiangsu, P. R. China

[‡]Institut für Chemie neuer Materialien, Universität Osnabrück, Barbarastrasse 7, 49076 Osnabrück, Germany

Supporting Information

ABSTRACT: Ideal membrane configurations for efficient separation at high flux rates consist of thin size-selective layers connected to macroporous supports for mechanical stabilization. We show that micelle-derived (MD) composite membranes combine efficient separation of similarly sized proteins and water flux 5−10 times higher than that of commercial membranes with similar retentions. MD composite membranes were obtained by filtration of solutions of amphiphilic block copolymer (BCP) micelles through commercially available macroporous supports covered by sacrificial nanostrand fabrics followed by annealing and removal of the nanostrand fabrics. Swelling-induced pore generation in the BCP films thus covering the macroporous supports yielded ∼210 nm thin nanoporous size-selective BCP layers with porosities in the 40% range tightly connected to the macroporous supports. Permselectivity and flux rates of the size-selective BCP layers were adjusted by the BCP mass deposited per membrane area and by proper selection of swelling times. The preparation methodology described here may pave the way for a modular assembly system allowing the design of tailored separation membranes.

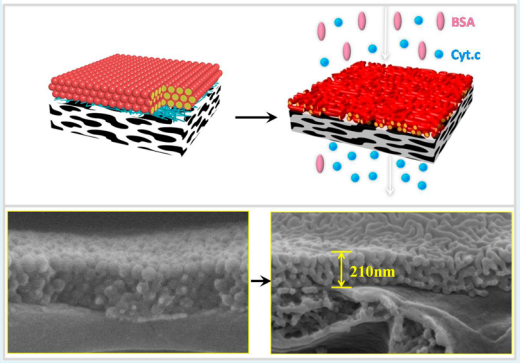

KEYWORDS: *separation, membranes, block copolymers, micelles, porous materials*

INTRODUCTION

Separation membranes are essential components in industry as well as in daily life and are relevant to fields as diverse as water treatment,[1] CO_2 capture,[2] and health care.[3] Recently, separation membranes exhibiting sharp separation selectivity were reported. For example, Yu et al. prepared free-standing fabrics of carbonaceous nanofibers by a hydrothermal carbonization process employing Te nanowires as templates.[4] A main challenge in the design of separation membranes is the optimization of hydraulic permeability and size-sieving performance in separation processes combined with mechanical stability and durability of the separation membranes. Mechanically stable size-selective layers with thicknesses in the micron range and above may be used as free-standing membranes but suffer from significant flow resistance. Ultrathin size-selective layers with thicknesses of a few 100 nm exhibit low flow resistance but suffer from poor mechanical stability and durability. Composite separation membranes consisting of a nanoporous size-sieving layer connected to a macroporous support may overcome these drawbacks. A major advantage of composite separation membranes is that size-sieving layers and macroporous supports can be designed independently. Ideally, nanoporous size-sieving layers with appropriate pore size and narrow pore size distribution are as thin as possible to reduce their flow resistance. The nanoporous size-sieving layers should be tightly attached to mechanically robust macroporous supports with negligible flow resistance.

So far, the preparation of composite membranes combining high selectivity and high flux with mechanical durability has remained challenging, in particular with respect to the coating of the macroporous supports with size-selective layers. Size-selective layers obtained by deposition of latex particles[5] or of fabrics of nanostrands[6] and nanofibers[7,8] onto macroporous supports typically suffer from insufficient mechanical stability and durability. Other previously reported preparation methods for composite separation membranes include, for example, interfacial polymerization[9,10] and direct coating.[11,12] However, interfacial polymerization yields dense films, which are only suitable for reverse osmosis and gas separation at low or modest flux under high operation pressures. Direct coating is also associated with drawbacks. Permeation of coating solutions into the macropores of the supports may result in coating of the macropore walls or even clogging of the macropores rather than in the formation of a thin size-selective layer on top of the support. The use of viscous coating solutions yields separation layers with thicknesses of to up to tens of micrometers so that the flux through the composite membranes is significantly

Received: February 2, 2015
Accepted: March 16, 2015
Published: March 16, 2015

DOI: 10.1021/acsami.5b01004
ACS Appl. Mater. Interfaces 2015, 7, 6974−6981

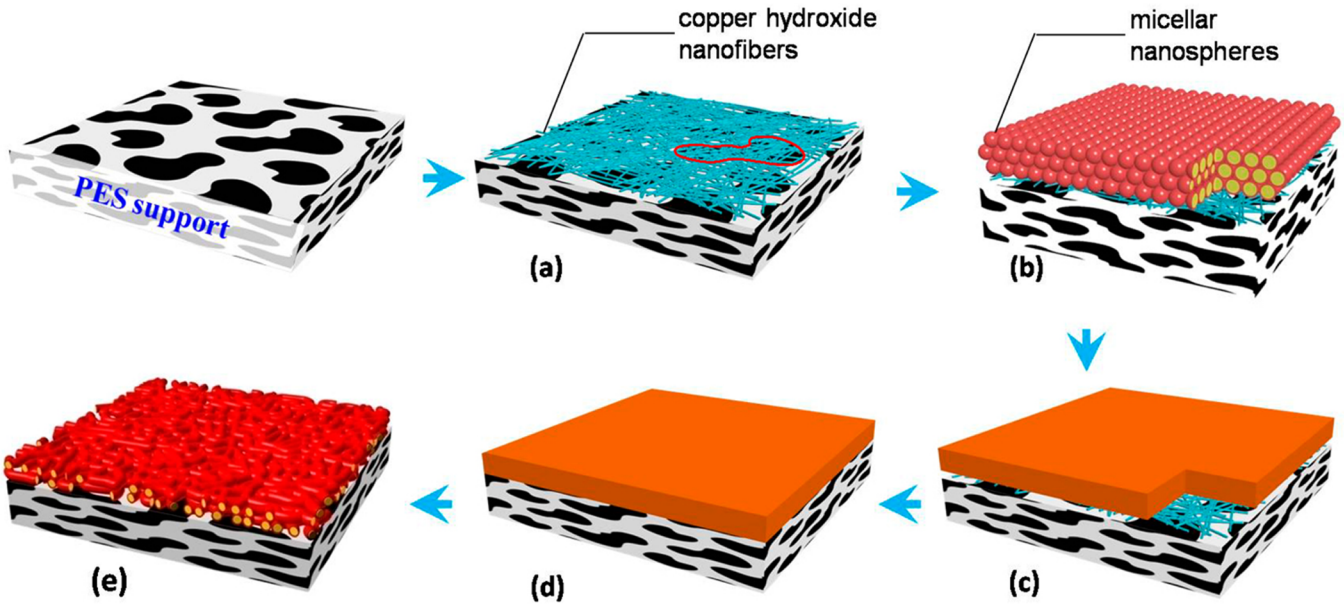

Figure 1. Preparation of MD composite membranes. (a) A sacrificial fabric of copper hydroxide nanostrands is deposited on a PES support by filtration. The contour of an exemplary macropore of the PES support is marked red. (b) PS-*b*-P2VP micelles are deposited on the layer of copper hydroxide nanostrands in a second filtration step. (c) The PS-*b*-P2VP micelles are fused by heating at 150 °C for 10 min. (d) The sacrificial layer of copper hydroxide nanostrands is dissolved using acetic acid. (e) Pores in the PS-*b*-P2VP layer are generated by swelling-induced pore generation.

reduced.[13] Synthetic protocols involving prefilling the macroporous supports with liquids immiscible with the coating solution as additional process step yield selective layers with thicknesses of a few micrometers.[11,14]

Here we report the generation of micelle-derived (MD) composite membranes that show sharp selectivity as well as low flow resistance and consist of ultrathin, nanoporous block copolymer (BCP) separation layers tightly connected to mechanically stable macroporous supports. The MD composite membranes were obtained by filtration of defined amounts of micellar solutions of the BCP through the macroporous support covered with a sacrificial fabric of nanostrands, followed by annealing, removal of the sacrificial nanostrand fabric, and swelling-induced pore generation in the BCP layer. Thus, BCP size-sieving layers with thicknesses of a few 100 nm and pore sizes of a few tens of nanometers are accessible that are characterized by the mechanical and chemical stability of polymers, their elasticity, and their low density.

RESULTS AND DISCUSSION

Preparation of Micelle-Derived Composite Membranes. The preparation of MD composite membranes is illustrated in Figure 1. As macroporous supports, we used poly(ether sulfone) (PES) microfiltration membranes with a nominal pore diameter of 450 nm (Supporting Information, Figure S1) and a thickness of ∼100 μm. The ultrathin nanoporous size-sieving layers consisted of asymmetric polystyrene-*block*-poly(2-vinylpyridine) (PS-*b*-P2VP), a highly amphiphilic BCP containing PS as major component and P2VP as minor component. Layers of PS-*b*-P2VP micelles served as precursors of the ultrathin nanoporous PS-*b*-P2VP size-sieving layers. However, since the PS-*b*-P2VP micelles had a uniform diameter of 60 nm,[15] which is smaller than the macropore size of the PES supports, it was not possible to deposit the PS-*b*-P2VP micelles directly on the PES supports. To overcome this problem, we deposited at first fabrics of nanostrands,[16] a class of one-dimensional inorganic nanostructures first reported in 2004,[17] on the PES supports. Adapting a procedure described elsewhere,[5,18] copper hydroxide nanostrand suspensions were filtrated through the PES supports to deposit fabrics of copper hydroxide nanostrands on their surfaces (Figure 1a; Supporting Information, Figure S2). Homogenous fabrics of copper hydroxide nanostrands prepared in the same way as in this work reject nanoparticles larger than 10 nm.[19,20] Hence, the fabrics of copper hydroxide nanostrands were dense enough to be nonpermeable to the PS-*b*-P2VP micelles. In the next step, defined amounts of a micellar PS-*b*-P2VP solution were filtrated through the PES supports covered with copper hydroxide nanostrand fabrics. In this way, composite membranes consisting of a PES support, an intermediate copper hydroxide nanostrand fabric, and PS-*b*-P2VP micelles as uppermost layer were obtained (Figure 1b). Heating for 10 min to 150 °C, a temperature well above the glass transition temperatures of PS and P2VP,[21] converted the PS-*b*-P2VP micelle layers into smooth and continuous PS-*b*-P2VP films (Figure 1c; Supporting Information, Figure S3). The intermediate layers of copper hydroxide nanostrands were then removed by treatment with aqueous acetic acid (Figure 1d). Finally, the smooth and continuous PS-*b*-P2VP layers on the PES supports were converted into ultrathin nanoporous size-sieving layers (Figure 1e) by swelling-induced pore generation.[22−26] In brief, the P2VP minority domains are selectively swollen with ethanol. The glassy PS majority domains undergo structural reconstruction to accommodate the increased volume of the swollen P2VP domains. Evaporation of the ethanol results in entropic relaxation of the extended P2VP chains, and pores form in place of the swollen P2VP domains. Swelling-induced pore generation resulted in the formation of tight adhesive contact between the ultrathin nanoporous PS-*b*-P2VP size-sieving layers and the macroporous PES supports.

Morphology of Micelle-Derived Composite Membranes. Figure 2 shows a composite membrane consisting of as-deposited PS-*b*-P2VP micelles covering a sacrificial copper hydroxide nanostrand fabric on a PES support prepared by

DOI: 10.1021/acsami.5b01004
ACS Appl. Mater. Interfaces 2015, 7, 6974−6981

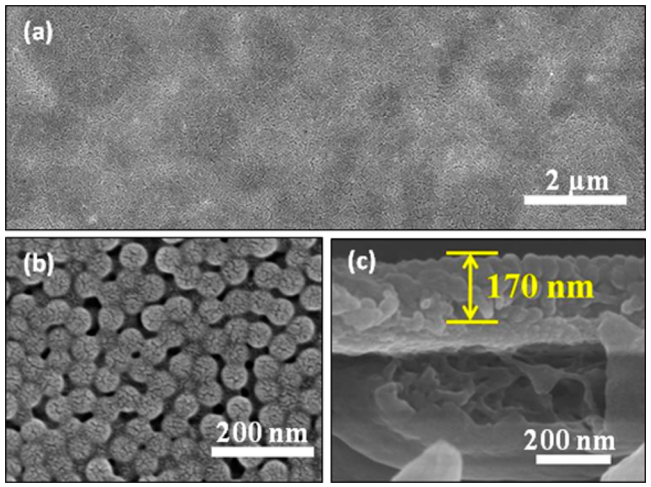

Figure 2. SEM images showing (a, b) top views and (c) a cross-sectional view of PS-*b*-P2VP micelles deposited on PES supports covered by copper hydroxide nanostrands. 14.7 μg of PS-*b*-P2VP/cm^2 of membrane area was deposited by proper control of the amount of filtrated PS-*b*-P2VP micelle solution.

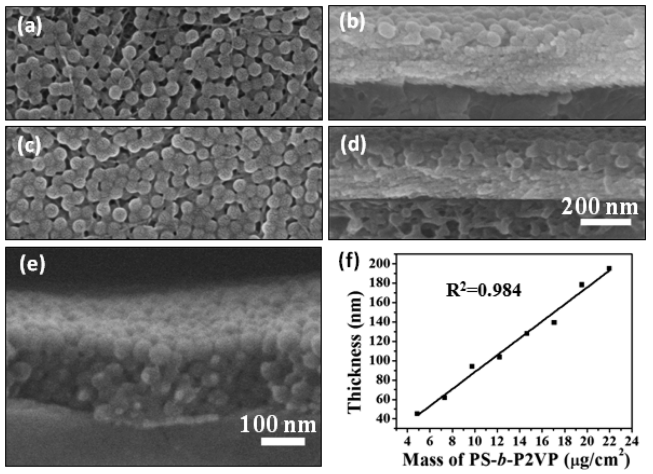

Figure 3. SEM images of (a, c) surfaces and (b, d, e) cross sections of PS-*b*-P2VP micelle layers prepared by filtration−deposition of different amounts of PS-*b*-P2VP on PES supports coated with copper hydroxide nanostrand fabrics. The amount of deposited PS-*b*-P2VP is quantified as mass of PS-*b*-P2VP per membrane area: (a, b) 4.9 μg/cm^2, (c, d) 9.8 μg/cm^2, and (e) 22.1 μg/cm^2. (f) Relationship between the thickness of the PS-*b*-P2VP layers after heating to 150 °C for 10 min and the mass PS-*b*-P2VP deposited per membrane area. The solid line is a linear fit.

deposition of 14.7 μg of PS-*b*-P2VP/cm^2 of membrane area. The PS-*b*-P2VP micelles form an even and uniform layer even at the positions of the macropores of the PES support layer (Figure 2a). The PS-*b*-P2VP layer consists of discrete, densely packed PS-*b*-P2VP micelles, some of which are tightly connected with their neighbors because of the fusing of P2VP coronae during drying (Figure 2b). The thickness of the micellar PS-*b*-P2VP layer of ∼170 nm was uniform across the sample (Figure 2c). In an ideal hexagonal lattice, a layer thickness of 170 nm would correspond to four stacked layers of PS-*b*-P2VP micelles.

The thickness of the PS-*b*-P2VP films on the copper hydroxide nanostrand fabrics after annealing to 150 °C for 10 min (cf. Figure 1c) can be adjusted by the amount of PS-*b*-P2VP deposited per membrane area, which can in turn be adjusted via the mass of PS-*b*-P2VP in the filtered micellar PS-*b*-P2VP solution. The copper hydroxide nanostrand fabrics were incompletely covered by PS-*b*-P2VP micelles when 4.9 μg of PS-*b*-P2VP/cm^2 of membrane area was deposited (Figure 3a,b). Deposition of 9.8 μg of PS-*b*-P2VP/cm^2 of membrane area, corresponding to 2−3 layers of PS-*b*-P2VP micelles, resulted in complete coverage (Figure 3c,d). Deposition of 22.1 μg of PS-*b*-P2VP/cm^2 of membrane area yielded four to five PS-*b*-P2VP micelle layers (Figure 3e). The thickness of the smooth PS-*b*-P2VP layers obtained by heating the as-deposited PS-*b*-P2VP micelle layers to 150 °C for 10 min was proportional to the mass of PS-*b*-P2VP deposited per membrane area (Figure 3f). Annealing of PS-*b*-P2VP micelle layers obtained by deposition of 14.7 μg of PS-*b*-P2VP/cm^2 of membrane area (cf. Figure 2) yielded a continuous PS-*b*-P2VP layer with a thickness of 128 nm (the annealed PS-*b*-P2VP layer was transferred onto a silicon wafer after removal of the copper hydroxide nanostrand fabric, and the thickness of the continuous PS-*b*-P2VP layer was determined by spectroscopic ellipsometry). The apparent decrease in thickness from 170 nm prior to annealing to 128 nm after annealing is presumably caused by densification, that is, the vanishing of the gaps between the PS-*b*-P2VP micelles upon melting. The heating time needs to be adjusted carefully. If the heating time is too short, the PS-*b*-P2VP micelles do not fuse. If the heating time is too long, the PS-*b*-P2VP will infiltrate the copper hydroxide nanostrand fabric or even the PES support.

In the final preparation step, nanopores are generated in the PS-*b*-P2VP layers by swelling-induced pore generation. If the parameters are properly selected, in this way continuous pore networks are formed. For example, we prepared continuous nanopore systems in micron-thick PS-*b*-P2VP membranes by swelling-induced pore generation with ethanol at 60 °C for 15 h. Then, we prepared replicas of the continuous nanopore systems by electroplating of gold. Elecron microscopy analysis of the gold replicas after dissolution of the PS-*b*-P2VP evidenced the continuous nature of the nanopore systems, which completely penetrated the micron-thick PS-*b*-P2VP membranes.[23] The bicontinuous nature of the PS-*b*-P2VP size-sieving layers is, for example, indeed obvious from the SEM image of an MD composite membrane with a PS-*b*-P2VP size-sieving layer obtained by deposition of 14.7 μg of PS-*b*-P2VP/cm^2 of membrane area and swelling-induced pore generation in ethanol at 55 °C for 15 h shown in Figure 4a. Closer SEM examination (Figure 4b) revealed that the nanopores had a mean width of 20 ± 4 nm and narrow channel-like shape. The cross-sectional SEM images shown in Figure 4c,d evidence that the nanopores form a network penetrating through the entire PS-*b*-P2VP layer. Swelling-induced pore generation was further studied by spectroscopic ellipsometry. For this purpose, a nonporous PS-*b*-P2VP layer formed by deposition of 14.7 μg of PS-*b*-P2VP/cm^2 of membrane area on a copper hydroxide nanostrand fabric was annealed, transferred onto a silicon wafer, and swollen in the same way as the PS-*b*-P2VP layers on the PES supports. Spectroscopic ellipsometry revealed an average thickness of the nanoporous PS-*b*-P2VP layer of 213 nm. This value is in excellent agreement with the thickness of the nanoporous PS-*b*-P2VP layers on macroporous PES supports apparent in SEM images (Figure 4c). The increase in thickness by ∼66% from 128 nm prior to swelling-induced pore generation to 213 nm after swelling-induced pore generation

DOI: 10.1021/acsami.5b01004
ACS Appl. Mater. Interfaces 2015, 7, 6974−6981

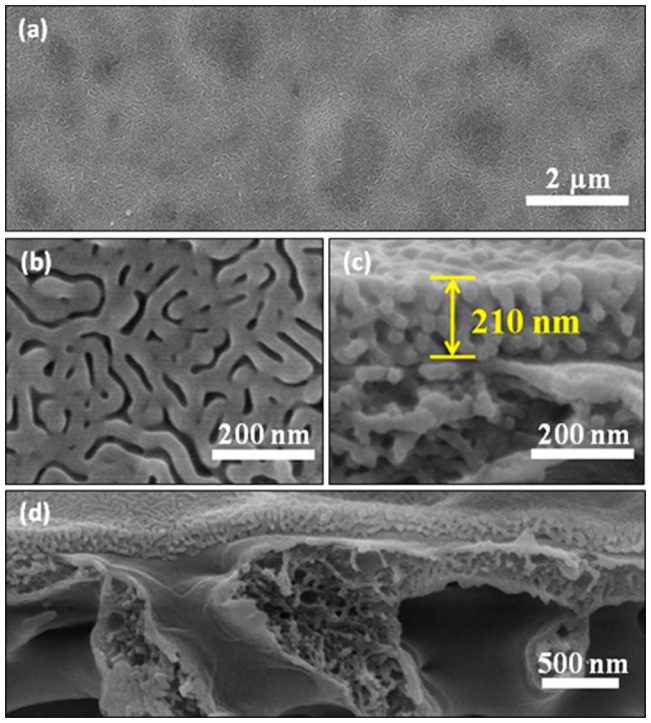

Figure 4. SEM images of MD composite membranes consisting of nanoporous PS-*b*-P2VP size-sieving layers on macroporous PES supports. The nanoporous PS-*b*-P2VP size-sieving layers were obtained by depositing 14.7 μg of PS-*b*-P2VP/cm^2 of membrane area, removal of the intermediate copper hydroxide nanostrand fabric, and swelling-induced pore generation in ethanol at 55 °C for 15 h. (a, b) Surface and (c, d) cross sections.

allows estimating the porosity of the nanoporous PS-*b*-P2VP size-sieving layers to ~40%.

Higher temperatures enhance both the affinity of ethanol to P2VP and the mobility of the PS chains. Hence, swelling-induced pore generation sensitively depends on the swelling temperatures. Subjecting a PS-*b*-P2VP layer obtained by deposition of 14.7 μg of PS-*b*-P2VP/cm^2 of membrane area to swelling-induced pore generation in ethanol for 1 h at 65 °C yielded a nanoporous PS-*b*-P2VP size-sieving layer with an apparent pore size of 27 ± 9 nm (Figure 5 a,b). The thickness of the PS-*b*-P2VP layer increased from 128 nm prior to swelling-induced pore generation to 239 nm after swelling-induced pore generation, as revealed by spectroscopic ellipsometry. The porosity estimated from the increase in

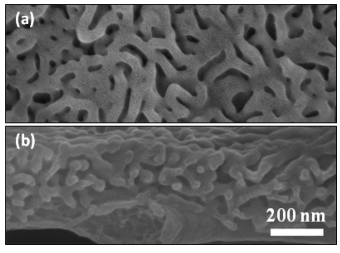

Figure 5. SEM images of (a) the surface and (b) a cross-section of a nanoporous PS-*b*-P2VP size-sieving layer on a macroporous PES support obtained by depositing 14.7 μg of PS-*b*-P2VP/cm^2 of membrane area, removal of the intermediate copper hydroxide nanostrand layer, and swelling-induced pore generation in ethanol at 65 °C for 1 h.

layer thickness amounted to ~46%. Hence, swelling-induced pore generation at 65 °C for 1 h yielded larger pores and higher porosities than swelling-induced pore generation at 55 °C for 15 h. In general, for a given swelling duration pore sizes and apparent porosities increase with increasing swelling temperature. After swelling-induced pore generation in ethanol for 1 h, at 50 °C a mean pore diameter of 16 ± 3 nm was reached. At 55 °C the pore size amounted to 18 ± 4 nm, at 58 °C to 19 ± 4 nm, at 60 °C to 21 ± 5 nm (Figure 6a–d; Figure 7a), and at 65 °C, as mentioned above, to 27 ± 9 nm (Figure 5a,b; Figure 7a).

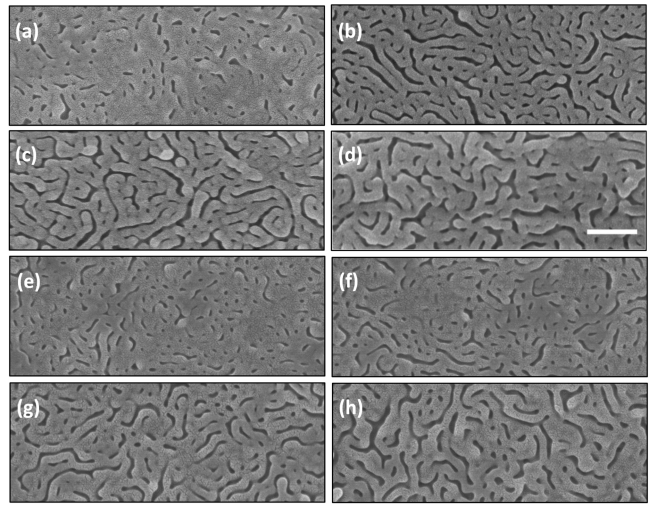

Figure 6. SEM images of nanoporous PS-*b*-P2VP size-sieving layers on macroporous PES supports obtained by depositing 14.7 μg of PS-*b*-P2VP/cm^2 of membrane area, removal of the intermediate copper hydroxide nanostrand layer, and swelling-induced pore generation in ethanol. (a–d) Swelling-induced pore generation for 1 h at temperatures of (a) 50, (b) 55, (c) 58, and (d) 60 °C. (e–h) Swelling-induced pore generation at 55 °C for (e) 10 min, (f) 30 min, (g) 4 h, and (h) 10 h. All SEM images have the same magnification. The scale bar in panel (d) corresponds to 200 nm.

The degree of morphology coarsening realized by swelling-induced pore generation can also be influenced by the applied swelling times. Figure 6e–h shows SEM images of nanoporous PS-*b*-P2VP size-sieving layers on macroporous PES supports obtained by depositing 14.7 μg of PS-*b*-P2VP/cm^2 of membrane area, removal of the intermediate copper hydroxide nanostrand layer, and swelling-induced pore generation in ethanol at 55 °C for different periods of time, whereas the evaluation results are summarized in Figure 7b. After 10 and 30 min, nanopores with mean pore widths of 14 ± 3 nm and 17 ± 3 nm emerged (Figure 6e,f). After 4 h, the apparent pore size had slightly increased to 18 ± 3 nm (Figure 6g) and did not markedly change after six more hours swelling time (mean pore diameter 19 ± 4 nm; Figure 6h) and after overall 15 h swelling time (mean pore diameter 20 ± 4 nm; Figure 4b).

Independent of the conditions applied, swelling-induced pore generation led to the migration of P2VP blocks to the pore walls and the outer surface of the nanoporous PS-*b*-P2VP selective layers, as evidenced by XPS. As the P2VP chains contain one nitrogen atom per repeat unit, the 1s peak of nitrogen centering about 399 eV indicates the presence of nitrogen at the surface. The nitrogen 1s peak appeared in XPS spectra of the PS-*b*-P2VP layers (14.7 μg of PS-*b*-P2VP/cm^2 of membrane area) prior to and after swelling-induced pore

DOI: 10.1021/acsami.5b01004
ACS Appl. Mater. Interfaces 2015, 7, 6974–6981

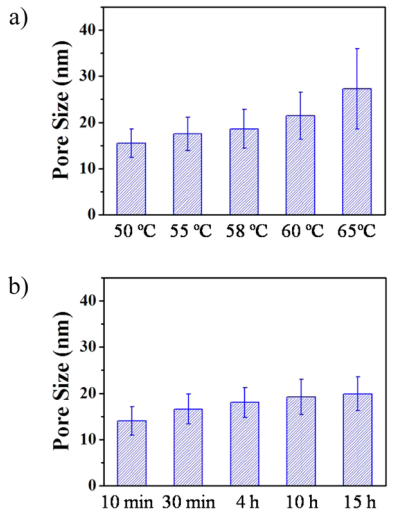

Figure 7. Mean pore diameters of nanoporous PS-*b*-P2VP size-sieving layers on macroporous PES supports obtained by depositing 14.7 μg of PS-*b*-P2VP/cm^2 of membrane area, removal of the intermediate copper hydroxide nanostrand layer, and swelling-induced pore generation in ethanol. The mean pore diameters were obtained by evaluation of at least 100 nanopores manually selected in SEM images of corresponding MD composite membranes using the software Nano Measurer. The standard deviations are indicated by error bars. (a) Mean nanopore diameters obtained by swelling-induced pore generation for 1 h in ethanol at different temperatures. (b) Mean nanopore diameters obtained by swelling-induced pore generation in ethanol at 55 °C for different periods of time.

generation (Figure 8). The atomic ratio of nitrogen to carbon (N/C) before swelling-induced pore generation amounted to

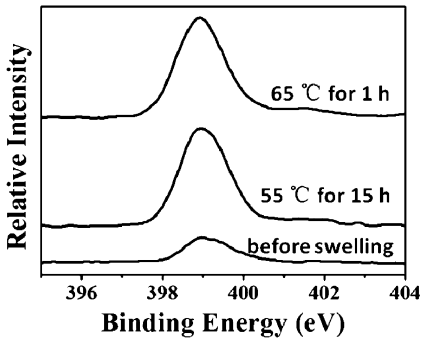

Figure 8. XPS spectra of the surfaces of nanoporous PS-*b*-P2VP layers after swelling-induced pore generation and of solid PS-*b*-P2VP layers prior to swelling-induced pore generation obtained by deposition of 14.7 μg of PS-*b*-P2VP/cm^2 of membrane area. The XPS spectra show the region of the N 1s peaks.

1.6%, whereas the N/C ratio increased to 6.7−6.8% after swelling-induced pore generation at 55 °C for 15 h and at 65 °C for 1 h. The increase in the N/C ratio indicates that the higher affinity of P2VP to the solvent ethanol as compared to PS pushes the P2VP blocks to the surface of the nanoporous PS-*b*-P2VP size-sieving layers. These results are in line with results of electron microscopy investigations reported previously.[22,27]

Performance of Micelle-Derived Composite Membranes. We investigated the permselectivity of MD composite membranes prepared by swelling-induced pore generation in the PS-*b*-P2VP size-sieving layer for different periods of time and at different temperatures. The bare PES support had a pure water flux (PWF) of 58 400 L·m^{-2}·h^{-1}·bar^{-1} and a negligible retention to BSA. Flux and retention properties of MD composite membranes sensitively depended on swelling times. Figure 9a shows the PWF and BSA retention of MD composite

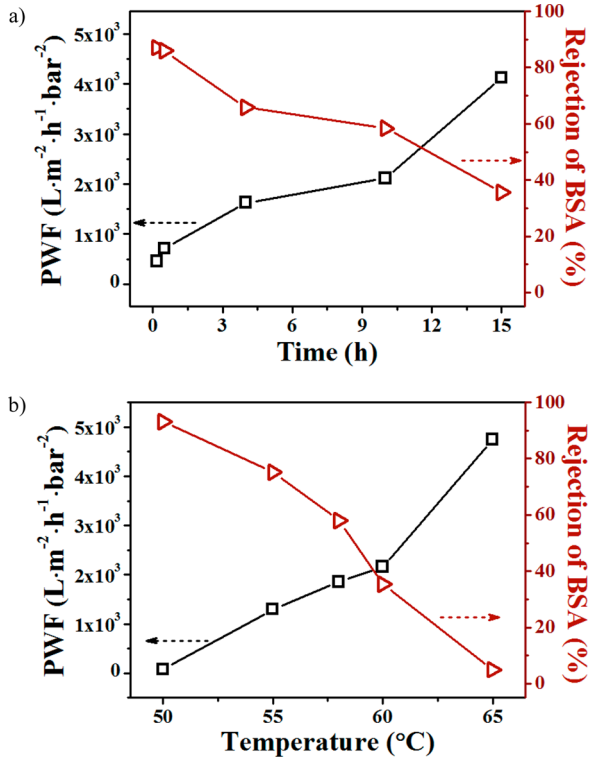

Figure 9. PWF and BSA retention of MD composite membranes with selective PS-*b*-P2VP layers (14.7 μg of PS-*b*-P2VP/cm^2 of membrane area) prepared (a) by swelling-induced pore generation at 55 °C for different periods of time and (b) by swelling-induced pore generation for 1 h at different temperatures. The solid lines connecting the data points are guides to the eyes.

membranes (14.7 μg of PS-*b*-P2VP/cm^2 of membrane area) prepared by swelling-induced pore generation at 55 °C for different periods of time. Swelling-induced pore generation for 10 min resulted in a PWF of 452 L·m^{-2}·h^{-1}·bar^{-1} and a BSA retention of 87%. For a swelling duration of 30 min, the PWF remarkably increased to 710 L·m^{-2}·h^{-1}·bar^{-1}, while the BSA retention still reached 86%. Increasing the swelling time to 4 h, 10 h, and 15 h resulted in further increasing PWF values of 1627, 2111, and 4123 L·m^{-2}·h^{-1}·bar^{-1}, but the BSA retention decreased from 66% to 58% to 36%, respectively. These results are consistent with the observation that pore size and porosity increase with increasing swelling time. However, because of the small thickness of the selective PS-*b*-P2VP layer in the 200 nm range, configurations are accessible that combine high PWF values with high retention. For example, the PWF value of 710 L·m^{-2}·h^{-1}·bar^{-1} of MD composite membranes obtained by swelling the selective PS-*b*-P2VP layer for 30 min at 55 °C was 5−10 times higher than that of typical commercial ultrafiltration membranes with a molecular weight cutoff of 50 kDa (PWF ≈ 60−130 L·m^{-2}·h^{-1}·bar^{-1}).[28] The PWF value was also 5 times higher than that of comparable membranes having nanoporous PS-*b*-P2VP size-sieving layers with thicknesses of several micrometers directly coated on macroporous supports.[14]

DOI: 10.1021/acsami.5b01004
ACS Appl. Mater. Interfaces 2015, 7, 6974−6981

The same trends as for increased swelling times at a given temperature were evident in the performance tests of MD composite membranes with PS-*b*-P2VP size-sieving layers (14.7 μg of PS-*b*-P2VP/cm^2 of membrane area) swollen for 1 h at different swelling temperatures (Figure 9b). A swelling temperature of 50 °C yielded a PWF of 76 L·m^{-2}·h^{-1}·bar^{-1} and a BSA retention of 93%, a swelling temperature of 55 °C yielded a PWF of 1294 L·m^{-2}·h^{-1}·bar^{-1} and a BSA retention of 75%, a swelling temperature of 58 °C yielded a PWF of 1852 L·m^{-2}·h^{-1}·bar^{-1} and a BSA retention of 58%, and a swelling temperature of 60 °C yielded a PWF of 2161 L·m^{-2}·h^{-1}·bar^{-1} and a BSA retention of 35%. Swelling at 65 °C for 1 h yielded a PWF of 4744 L·m^{-2}·h^{-1}·bar^{-1} but a BSA retention of only 5%. Already slight increases in the swelling temperature result in significant increases in the PWF but also in significant decreases in the BSA retention. Thus, slight temperature changes strongly influence swelling-induced pore generation and, consequently, separation performance of the PS-*b*-P2VP size-sieving layers. BSA adsorption on the composite membranes[14] was negligible. The low degree of BSA absorption is presumably caused by the high hydrophilicity of the P2VP chains at the surfaces of the PS-*b*-P2VP size-sieving layers.[29,30] Hence, BSA retention was exclusively based on size discrimination controlled by the sizes of the pores in the PS-*b*-P2VP size-sieving layers.

Ultrafiltration membranes typically require a 10-fold difference in molecular mass between the species to be separated to obtain effective separation.[31] However, MD composite membranes show sharp separation selectivity in the separation of similarly sized proteins, such as bovine serum albumin (BSA) and cytochrome C (Cyt. C). BSA has a molecular weight of 67 000 Da and molecular dimensions of 14 nm × 3.8 nm × 3.8 nm,[31] whereas Cyt. C has a molecular weight of 14 000 Da and a molecular volume of 2.5 nm × 2.5 nm × 3.7 nm.[32] We used an aqueous mixture that initially contained BSA and Cyt. C at concentrations of 0.5 g/L and 0.02 g/L corresponding to a protein mass ratio ($m_{BSA}/m_{Cyt.C}$) of 25. Filtration through an MD composite membrane obtained by deposition of 14.7 μg of PS-*b*-P2VP/cm^2 of membrane area and swelling-induced pore generation in ethanol for 30 min at 55 °C revealed retentions of BSA and Cyt. C of ∼90% and ∼30%, respectively (Figure 10). Hence, 10% of the BSA molecules and 70% of the Cyt. C molecules in the feed passed the MD composite membrane. As a result, in the concentrate $m_{BSA}/m_{Cyt.C}$ increased from 25 to 36.5 after half of the volume of the feed had passed the MD composite membrane; BSA enriched in the concentrate, while most of the Cyt. C molecules passed the MD composite membrane and enriched in the filtrate. The smaller Cyt. C molecules were efficiently separated from the mixture because the PS-*b*-P2VP size-sieving layer has apparently a narrow pore size distribution.

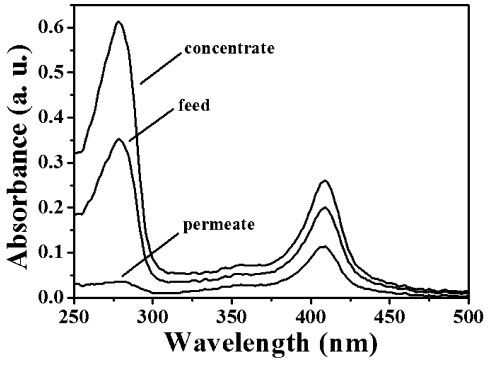

Figure 10. UV−vis spectra of feed, permeate, and concentrate after filtration of an aqueous mixture of BSA and Cyt. C (see main text) through an MD composite membrane obtained by deposition of 14.7 μg of PS-*b*-P2VP/cm^2 of membrane area and swelling-induced pore generation in ethanol for 30 min at 55 °C. The peak at 280 nm is characteristic of BSA, while the peak at 409 nm is characteristic of Cyt. C.

Stability of Micelle-Derived Composite Membranes. In general, nanoporous PS-*b*-P2VP layers prepared by swelling-induced pore generation show excellent mechanical stability. For example, nanoporous PS-*b*-P2VP supports bearing arrays of likewise nanoporous PS-*b*-P2VP nanorods were used as bioinspired adhesive systems[33,34] that showed constant adhesion performance in series of adhesion tests successively performed under different relative humidities.[33] Indeed, the MD composite membranes showed no noticeable drop in PWF under long-term operation. For example, Figure 11 shows PWF

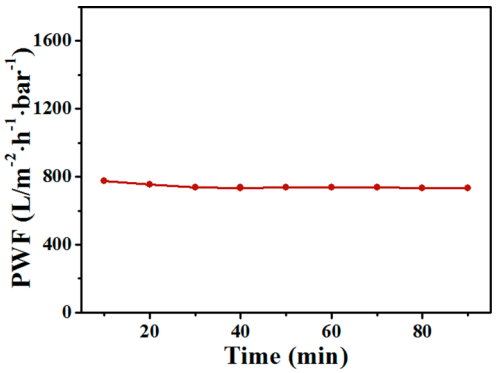

Figure 11. PWF as a function of filtration time of an MD composite membrane with 14.7 μg of PS-*b*-P2VP/cm^2 of membrane area prepared by swelling-induced pore generation at 55 °C for 30 min. The solid line connecting the data points is a guide to the eyes.

values captured during filtration for 90 min using an MD composite membrane with 14.7 μg of PS-*b*-P2VP/cm^2 of membrane area prepared by swelling-induced pore generation at 55 °C for 30 min. The PWF value at t = 10 min amounted to 776 L·m^{-2}·h^{-1}·bar^{-2}, and that at t = 90 min amounted to 734 L·m^{-2}·h^{-1}·bar^{-2}. The BSA rejection after filtration for 90 min amounted to ∼94%. The adhesion of the PS-*b*-P2VP size-sieving layers to the PES supports was so strong that the MD composite membranes withstood back flushing. After back flushing at 0.02 MPa for 3 min, an MD composite membrane with 14.7 μg of PS-*b*-P2VP/cm^2 of membrane area prepared by swelling-induced pore generation at 55 °C for 30 min still showed a BSA rejection of 93%.

CONCLUSIONS

Micelle-derived composite membranes were obtained by filtrating defined amounts of micellar solutions of amphiphilic BCPs through macroporous supports covered with sacrificial nanostrand fabrics. Annealing and removal of the sacrificial nanostrand fabrics followed by swelling-induced pore generation yielded ultrathin nanoporous BCP size-sieving layers with a thickness of a few 100 nm tightly connected to the mechanically stable macroporous supports. Selection of the BCP, the amount of BCP deposited per membrane area, and duration of as well as temperature during swelling-induced pore generation, allow precise adjustment of the properties of the

DOI: 10.1021/acsami.5b01004
ACS Appl. Mater. Interfaces 2015, 7, 6974−6981

BCP size-sieving layers. Therefore, mechanically stable configurations combining high flux and high selectivity are accessible by filtration-based syntheses of MD composite membranes. Because of the ultrathin and highly porous nature of the BCP size-sieving layer, the MD composite membranes may exhibit 5−10 times higher permeability than commercial ultrafiltration membranes with similar retentions. MD composite membranes enable efficient separation of proteins with similar sizes. Filtration-based synthesis of MD separation membranes is a synthetic modular assembly system allowing the design of tailor-made membrane configurations for a broad range of separation problems.

METHODS

Materials. PS-*b*-P2VP (M_n(PS) = 50 000 g mol^{-1}; M_n(P2VP) =16 500 g mol^{-1}, M_w/M_n (PS-*b*-P2VP) = 1.09) was purchased from Polymer Source Inc., Canada, and used without further purification. Aminoethanol ($NH_2CH_2CH_2OH$), BSA with a purity of >97%, and cytochrome C with a purity of >95% were obtained from Sigma-Aldrich. Analytical reagent-grade copper nitrate ($Cu(NO_3)_2{\cdot}3H_2O$), acetic acid, sodium hydroxide, and ethanol were purchased from local suppliers and used as received. PES microfiltration membranes were purchased from Tianjin Jinteng Instrument Co. Ltd. in the form of circular chips with a diameter of 2.5 cm. Copper hydroxide nanostrands with diameters less than 10 nm and lengths up to 10 μm (Supporting Information, Figure S2) were synthesized as described in the literature.[35] Briefly, 250 mL of an aqueous solution of $Cu(NO_3)_2$ (4 mmol/L) was mixed with 250 mL of an aqueous solution of aminoethanol (4 mmol/L). The mixture was moderately stirred at room temperature for 2 min. Then, the solution was allowed to stand for 3 d.

Details of the Preparation of the Micelle-Derived Composite Membranes. A solution of 20 mg of PS-*b*-P2VP dissolved in 10 g of acetic acid was kept at 110 °C for 15 h to form PS-*b*-P2VP micelles.[15] The micellar solution was cooled to room temperature and diluted 10 times with ethanol. The solution was neutralized by adding an equal volume of 7 wt % sodium hydroxide solution, because acidic solutions would destroy the copper hydroxide nanostrands, and unwanted precipitation of the PS-*b*-P2VP micelles is prevented in this way.[36] Finally, the mixture was further diluted five times with ethanol.

Macroporous PES supports were soaked in deionized water for 10 min and then fixed in a glass vacuum filter holder (16306, Sartorius AG). The pores of the PES supports were then wetted with 10 g of deionized water. To deposit layers of copper hydroxide nanostrands on the surfaces of the PES supports, 10 g of the copper hydroxide nanostrand suspension was filtrated through the PES supports (Figure 1a). Then, defined amounts of the micellar PS-*b*-P2VP solution ranging from 1.0 to 4.5 g were filtrated through the PES supports covered with copper hydroxide nanostrands at a pressure of 5 kPa (Figure 1b). After heating for 10 min at 150 °C, the intermediate layers of copper hydroxide nanostrands were removed by treatment with 1 wt % aqueous acetic acid for 10 min, followed by heating to 50 °C to enhance the adhesion between the PS-*b*-P2VP films and the PES supports (Figure 1d). Swelling-induced pore generation in the PS-*b*-P2VP film was carried out with ethanol at selected temperatures for selected periods of time.

Characterization. Scanning electron microscopy (SEM) investigations on samples sputter-coated with Au/Pd alloy were performed with a field emission SEM Hitachi S4800 operated at 5 kV. Cross-sectional specimens were prepared by fracturing in liquid nitrogen. Frequency densities of the nanopore diameters were obtained by evaluation of at least 100 nanopores manually selected in SEM images of the MD composite membranes using the software Nano Measurer. The thickness of the PS-*b*-P2VP layers (before pore generation) was measured with a spectroscopic ellipsometer (Complete EASE M-2000U, J. A. Woollam) using a laser with a wavelength of 632.8 nm at an incident angle of 70°. For this purpose, PS-*b*-P2VP films coated on PES supports were transferred on silicon wafers after etching the sacrificial copper hydroxide nanostrand fabrics. X-ray photoelectron spectroscopy (XPS) was performed with an ESCALAB 250 XPS system (Thermo Scientific) using a monochromatic Al Kα X-ray source. To compensate the surface charge effects, all binding energies in the spectra were referenced to the C 1s neutral peak at 285.0 eV.

Filtration and Separation Tests. Water flux as well as retention of BSA and Cyt. C were determined using a stirred filtration cell (Amicon Model 8003, Millipore Co., Billerica, MA) under a pressure of 0.02 MPa. For retention tests, BSA and Cyt. C were dissolved in phosphate buffer (pH = 7.4) at concentrations of 0.5 g/L and 0.02 g/L, respectively. Retention rates for BSA and Cyt. C were determined by measuring the concentrations of BSA and Cyt. C in solution using a NanoDROP 2000C UV−vis spectrometer (Thermo Scientific). For this purpose, we evaluated the relative intensities of the characteristic BSA peak at 280 nm and of the characteristic Cyt. C peak at 409 nm.

ASSOCIATED CONTENT

Supporting Information

SEM image of a PES support; SEM image of a copper hydroxide nanostrand fabric deposited on a PES support; SEM image of the surface of a PS-*b*-P2VP layer obtained by deposition of 22.1 μg of PS-*b*-P2VP/cm^2 of membrane area followed by annealing. This material is available free of charge via the Internet at http://pubs.acs.org.

AUTHOR INFORMATION

Corresponding Authors

*E-mail: yongwang@njtech.edu.cn. (Y.W.)
*E-mail: martin.steinhart@uni-osnabrueck.de. (M.S.)

Notes

The authors declare no competing financial interest.

ACKNOWLEDGMENTS

Financial support from the National Basic Research Program of China (2015CB655301), the Doctoral Program Foundation of Institutions of Higher Education of China (20123221110003), the Jiangsu Natural Science Funds for Distinguished Young Scholars (BK2012039), and the Jiangsu Science and Technology Pillaring Program (BE2013128) is gratefully acknowledged. X.Y, L.G, M.S., and Y.W. thank the Alexander von Humboldt Foundation for support through the Research Group Linkage Program.

DOI: 10.1021/acsami.5b01004
ACS Appl. Mater. Interfaces 2015, 7, 6974−6981

REFERENCES

(1) Elimelech, M.; Phillip, W. A. The Future of Seawater Desalination: Energy, Technology and The Environment. *Science* **2011**, *333*, 712−717.

(2) Carta, M.; Malpass-Evans, R.; Croad, M.; Rogan, Y.; Jansen, J. C.; Bernardo, P.; Bazzarelli, F.; McKeown, N. B. An Efficient Polymer Molecular Sieve for Membrane Gas Separations. *Science* **2013**, *339*, 303−307.

(3) Gultepe, E.; Nagesha, D.; Sridhar, S.; Amiji, M. Nanoporous Inorganic Membranes or Coatings for Sustained Drug Delivery in Implantable Devices. *Adv. Drug Delivery Rev.* **2010**, *62*, 305−315.

(4) Liang, H. W.; Wang, L.; Chen, P. Y.; Lin, H. T.; Chen, L. F.; He, D.; Yu, S. H. Carbonaceous Nanofiber Membranes for Selective Filtration and Separation of Nanoparticles. *Adv. Mater.* **2010**, *22*, 4691−4695.

(5) Ramakrishnan, S.; McDonald, C. J.; Prud'homme, R. K.; Carbeck, J. D. Latex Composite Membranes: Structure and Properties of The Discriminating Layer. *J. Membr. Sci.* **2004**, *231*, 57−70.

(6) Peng, X. S.; Jin, J.; Ichinose, I. Mesoporous Separation Membranes of Polymer-Coated Copper Hydroxide Nanostrands. *Adv. Funct. Mater.* **2007**, *17*, 1849−1855.

(7) Ma, H. Y.; Burger, C.; Hsiao, B. S.; Chu, B. Ultrafine Polysaccharide Nanofibrous Membranes for Water Purification. *Biomacromolecules* **2011**, *12*, 970−976.

(8) Yao, X. P.; Wang, Z. G.; Yang, Z. M.; Wang, Y. Energy-saving, Responsive Membranes with Sharp Selectivity Assembled From Micellar Nanofibers of Amphiphilic Block Copolymers. *J. Mater. Chem. A* **2013**, *1*, 7100−7110.

(9) Lau, W. J.; Ismail, A. F.; Misdan, N.; Kassim, M. A. A Recent Progress in Thin Film Composite Membrane: A Review. *Desalination* **2012**, *287*, 190−199.

(10) Chen, H. M.; Hung, W. S.; Lo, C. H.; Huang, S. H.; Cheng, M. L.; Liu, G.; Lee, K. R.; Lai, J. Y.; Sun, Y. M.; Hu, C. C.; Suzuki, R.; Ohdaira, T.; Oshima, N.; Jean, Y. C. Free-Volume Depth Profile of Polymeric Membranes Studied by Positron Annihilation Spectroscopy: Layer Structure From Interfacial Polymerization. *Macromolecules* **2007**, *40*, 7542−7557.

(11) Phillip, W. A.; O'Neill, B.; Rodwogin, M.; Hillmyer, M. A.; Cussler, E. L. Self-Assembled Block Copolymer Thin Films as Water Filtration Membranes. *ACS Appl. Mater. Interfaces* **2010**, *2*, 847−853.

(12) Jahanshahi, M.; Rahimpour, A.; Peyravi, M. Developing Thin Film Composite Poly(piperazine-amide) and Poly(vinyl-alcohol) Nanofiltration Membranes. *Desalination* **2010**, *257*, 129−136.

(13) Jana, S.; Purkait, M. K.; Mohanty, K. Clay Supported Polyvinyl Acetate Coated Composite Membrane by Modified Dip Coating Method: Application for The Purification of Lysozyme from Chicken Egg White. *J. Membr. Sci.* **2011**, *382*, 243−251.

(14) Wang, Z. G.; Yao, X. P.; Wang, Y. Swelling-Induced Mesoporous Block Copolymer Membranes with Intrinsically Active Surfaces for Size-Selective Separation. *J. Mater. Chem.* **2012**, *22*, 20542−20548.

(15) Yang, Z. M.; Wang, Z. G.; Yao, X. P.; Wang, Y. Water-Dispersible, Uniform Nanospheres by Heating-Enabled Micellization of Amphiphilic Block Copolymers in Polar Solvents. *Langmuir* **2012**, *28*, 3011−3017.

(16) Karan, S.; Wang, Q. F.; Samitsu, S.; Fujii, Y.; Ichinose, I. Ultrathin Free-Standing Membranes from Metal Hydroxide Nanostrands. *J. Membr. Sci.* **2013**, *448*, 270−291.

(17) Ichinose, I.; Kurashima, K.; Kunitake, T. Spontaneous Formation of Cadmium Hydroxide Nanostrands in Water. *J. Am. Chem. Soc.* **2004**, *126*, 7162−7163.

(18) Yu, Q.; Huang, H. W.; Chen, R.; Yang, H. S.; Peng, X. S. Filtration-Assembling Colloidal Crystal Templates for Ordered Macroporous Nanoparticle Films. *J. Mater. Chem.* **2011**, *21*, 18089−18094.

(19) Shi, L.; Yu, Q.; Huang, H. B.; Mao, Y. Y.; Lei, J. H.; Ye, Z. Z.; Peng, X. S. Superior Separation Performance of Ultrathin Gelatin Films. *J. Mater. Chem. A* **2013**, *1*, 1899−1906.

(20) Peng, X. S.; Jin, J.; Ericsson, E. M.; Ichinose, I. General Method for Ultrathin Free-Standing Films of Nanofibrous Composite Materials. *J. Am. Chem. Soc.* **2007**, *129*, 8625−8633.

(21) *Polymer Handbook;* Brandrup, J., Immergut, E. H., Grulke, E. A., Abe, A., Bloch, D. R., Eds.; John Wiley and Sons: New York, 1999.

(22) Wang, Y.; Gösele, U.; Steinhart, M. Mesoporous Block Copolymer Nanorods by Swelling-Induced Morphology Reconstruction. *Nano Lett.* **2008**, *8*, 3548−3553.

(23) Wang, Y.; He, C. C.; Xing, W. H.; Li, F. B.; Tong, L.; Chen, Z. Q.; Liao, X. Z.; Steinhart, M. Nanoporous Metal Membranes with Bicontinuous Morphology from Recyclable Block Copolymer Templates. *Adv. Mater.* **2010**, *22*, 2068−2072.

(24) Wang, Y.; Li, F. B. An Emerging Pore-Making Strategy: Confined Swelling-Induced Pore Generation in Block Copolymer Materials. *Adv. Mater.* **2011**, *23*, 2134−2148.

(25) Yin, J.; Yao, X. P.; Liou, J. Y.; Sun, W.; Sun, Y. S.; Wang, Y. Membranes with Highly Ordered Straight Nanopores by Selective Swelling of Fast Perpendicularly Aligned Block Copolymers. *ACS Nano* **2013**, *7*, 9961−9974.

(26) Xue, L. J.; Kovalev, A.; Dening, K.; Eichler-Volf, A.; Eickmeier, H.; Haase, M.; Enke, D.; Steinhart, M.; Gorb, S. N. Reversible Adhesion Switching of Porous Fibrillar Adhesive Pads by Humidity. *Nano Lett.* **2013**, *13*, 5541−5548.

(27) Wang, Y.; Tong, L.; Steinhart, M. Swelling-Induced Morphology Reconstruction in Block Copolymer Nanorods: Kinetics and Impact of Surface Tension during Solvent Evaporation. *ACS Nano* **2011**, *5*, 1928−1938.

(28) GE MW Ultrafiltration (UF) Membrane, Sepa CF Size, from http://www.sterlitech.com/flat-sheet-membranes-specifications.html#UF. Accessed on July 9, 2014.

(29) Orlov, M.; Tokarev, I.; Scholl, A.; Doran, A.; Minko, S. pH-Responsive Thin Film Membranes from Poly (2-vinylpyridine): Water Vapor-Induced Formation of A Microporous Structure. *Macromolecules* **2007**, *40*, 2086−2091.

(30) Tokareva, I.; Minko, S.; Fendler, J. H.; Hutter, E. Nanosensors Based on Responsive Polymer Brushes and Gold Nanoparticle Enhanced Transmission Surface Plasmon Resonance Spectroscopy. *J. Am. Chem. Soc.* **2004**, *126*, 15950−15951.

(31) Striemer, C. C.; Gaborski, T. R.; McGrath, J. L.; Fauchet, P. M. Charge- and Size-Based Separation of Macromolecules Using Ultrathin Silicon Membranes. *Nature* **2007**, *445*, 749−753.

(32) Peng, X. S.; Jin, J.; Nakamura, Y.; Ohno, T.; Ichinose, I. Ultrafast Permeation of Water Through Protein-Based Membranes. *Nat. Nanotechnol.* **2009**, *4*, 353−357.

(33) Xue, L.; Kovalev, A.; Dening, K.; Eichler-Volf, A.; Eickmeier, H.; Haase, M.; Enke, D.; Steinhart, M.; Gorb, S. N. Reversible Adhesion Switching of Porous Fibrillar Adhesive Pads by Humidity. *Nano Lett.* **2013**, *13*, 5541−5548.

(34) Xue, L.; Kovalev, A.; Eichler-Volf, A.; Steinhart, M.; Gorb, S. N. Humidity-enhanced wet adhesion on insect-inspired fibrillar adhesive pads. *Nat. Commun.* **2015**, *6*, 6621.

(35) Luo, Y. H.; Huang, J. G.; Jin, J. A.; Peng, X. S. Formation of Positively Charged Copper Hydroxide Nanostrands and Their Structural Characterization. *Chem. Mater.* **2006**, *18*, 1795−1802.

(36) Yang, Z. M.; Wang, Z. G.; Yao, X. P.; Chen, Z. Q.; Wang, Y. Responsive, Fluorescent Micellar Nanospheres of Amphiphilic Block Copolymers for The Characterization of Membrane Pores. *J. Membr. Sci.* **2013**, *441*, 9−17.

DOI: 10.1021/acsami.5b01004
ACS Appl. Mater. Interfaces 2015, 7, 6974−6981